DFTT 68/93
November 1993

Five Jet Production with heavy quarks at e^+e^- Colliders [1]

Alessandro Ballestrero and Ezio Maina

Dipartimento di Fisica Teorica, Università di Torino
and INFN, Sezione di Torino
v. Giuria 1, 10125 Torino, Italy.

Abstract

Heavy quark production in five jet events at e^+e^- colliders is studied at tree level using helicity amplitudes. Total production rates for $2b3j$ and $4bj$ are given and compared with the corresponding results for massless quarks. The process $e^+e^- \to q\bar{q}gg\gamma$ which is the dominant contribution to $4j\gamma$ production is briefly discussed.

[1] Work supported in part by Ministero dell' Università e della Ricerca Scientifica.
e–mail: ballestrero,maina@to.infn.it

Introduction

The great number of hadronic decays of the Z^0 observed at LEP provides the opportunity to test our understanding of strong interactions in unprecedented detail. Large samples of multi–jet events have been accumulated and analyzed [1, 2]. In particular the ALEPH Collaboration and the OPAL Collaboration have studied the jet–fraction distributions as a function of y_{cut} for up to five jets.

Recent advances in b–tagging techniques based on the introduction of vertex detectors and on a refinement of the selection procedures, with their large efficiencies and the resulting high purities, have paved the way to the study of heavy–quark production in association with light–quark and gluon jets. The flavour independence of the strong coupling constant has been verified by several groups [3] using both jet–rates and shape variables.

It has been lately pointed out [4, 5] that the effects of the b–quark mass are substantial and increase with the number of jets.

In this paper we plan to study heavy–quark production in five–jet events at e^+e^- colliders. Two different mechanisms contribute to five–jet production for light quarks, the 'point–like' annihilation of e^+e^- to Z^0, γ [6], which dominates at LEP I energy, and W^+W^- production [7], followed by the emission of a gluon from the decay products of the W's, which dominates above the WW treshold. This latter contribution is severely suppressed for b–quarks by the smallness of the V_{bc} element of the CKM matrix and by the large mass of the *top* and will not be considered here. We have studied the annihilation mechanism for five–jet production at tree level taking full account of γ, Z interference and of quark masses. Therefore our matrix elements can be used at all e^+e^- colliders.

As a byproduct of the main calculation we have also examined the dominant contribution, $e^+e^- \to q\bar{q}gg\gamma$, to the production of a single hard photon in association with four jets. Both initial state and final state radiation have been included at tree level, without ISR resummation.

We have computed all matrix elements both in the formalism of [8, 9] and in that of [10] using the former for the actual calculation. The relevant formulae are summarized in the following section. Both methods can be easily implemented in a small set of nested subroutines. This however results in a computer program which is far too slow for the present calculation. We have instead used the symbolic package *Mathematica* [11] to write down the Fortran expression for each helicity amplitude. The individual Z-functions are computed first and then combined in larger structures that describe chunks of increasing size of the Feynman diagrams shown in fig.1–2. Every sub–diagram is saved and then used several times. With this procedure we have produced a rather large piece of code, which however runs quite fast, and therefeore can be used in high statistics Montecarlo runs. As an example the program for $q\bar{q}ggg$ production is about 24,000 lines long, but requires only about 5×10^{-2} seconds to evaluate on a Vaxstation 4000/90.

The amplitudes have been checked for gauge invariance. We have used $M_Z = 91.1$ GeV, $\Gamma_Z = 2.5$ GeV, $\sin^2(\theta_W) = .23$, $m_b = 5.$ GeV, $\alpha_{em} = 1/128$ and $\alpha_s = .115$ in the numerical part of our work.

Calculation

We present the helicity amplitudes in the formalism of [8, 9]. The two basic functions which are needed in writing the amplitudes are:

$$Z(p_i,\lambda_i;p_j,\lambda_j;p_k,\lambda_k;p_l,\lambda_l;c_R,c_L;c'_R,c'_L) = [\bar{u}(p_i,\lambda_i)\Gamma^{\mu}u(p_j,\lambda_j)][\bar{u}(p_k,\lambda_k)\Gamma'_{\mu}u(p_l,\lambda_l)] \tag{1}$$

where

$$\Gamma^{(\prime)\mu} = \gamma^{\mu}(c_R^{(\prime)}P_R + c_L^{(\prime)}P_L) \tag{2}$$

and

$$X(p_i,\lambda_i;p_j;p_k,\lambda_k) = [\bar{u}(p_i,\lambda_i)\not{p}_j\, u(p_k,\lambda_k)] \tag{3}$$

Their expressions in terms of spinor products $s(i,j) = \bar{u}(p_i,+)u(p_j,-) = t^*(j,i)$, η and μ functions can be found in Table I and II.

A convenient, though non unique, choice for the spinor products and for the functions η and μ is:

$$s(i,j) = (p_i^y + ip_i^z)\left(\frac{p_j^0 - p_j^x}{p_i^0 - p_i^x}\right)^{1/2} - (p_j^y + ip_j^z)\left(\frac{p_i^0 - p_i^x}{p_j^0 - p_j^x}\right)^{1/2} \tag{4}$$

$$\eta(i) = \left(2(p_i^0 - p_i^x)\right)^{1/2} \qquad \mu(i) = \pm\frac{m_i}{\eta(i)} \tag{5}$$

where the sign $+(-)$ refers to a particle (antiparticle) of mass m_i.

The polarization vectors of a gluon of momentum p_i can be written as

$$\varepsilon^{\mu}(p_i,\lambda) = N_i[\bar{u}(p_i,\lambda)\gamma^{\mu}u(p_{a(i)},\lambda)] \tag{6}$$

where $p_{a(i)}$ is an auxiliary massless momentum not parallel to p_i and the normalization factor is $N_i = [4(p_{a(i)}\cdot p_i)]^{-1/2}$. All amplitudes are independent of the $p_{a(i)}$'s.

There are fifty Feynman diagrams contributing to

$$e^-(p_1,\lambda) + e^+(p_2,-\lambda) \to q(p_6,\lambda_6) + \bar{q}(p_7,\lambda_7) + g(p_3,\lambda_3) + g(p_4,\lambda_4) + g(p_5,\lambda_5) \tag{7}$$

Some of them are shown in fig.1. All others can be obtained through permutations of the gluon labels. The two diagrams with four-gluon vertices are not shown. Their contribution is included in the expressions given below for the diagrams with two connected three–gluon vertices.

The amplitude squared for this process is:

$$\left|\overline{M}\right|^2_{q\bar{q}ggg} = \frac{1}{4}\frac{1}{3!}g_s^3e^2N_3N_4N_5\sum_{\{\lambda\}}\sum_{\pi,\pi'}M_{\pi}^{\{\lambda\}}M_{\pi'}^{\{\lambda\}*}C_{\pi\pi'} \tag{8}$$

where π is a permutation of the indexes $(3,4,5)$, $\{\lambda\}$ indicates the helicities of all external particles, M_π is the coefficient of the color matrix

$$T^{\pi}_{ij} = \left(T^{\pi(3)}T^{\pi(4)}T^{\pi(5)}\right)_{ij} \tag{9}$$

in the full amplitude and $C_{\pi\pi'}$ is the appropriate color factor, $C_{\pi\pi'} = \mathrm{Tr}(T^{\pi}(T^{\pi'})^{\dagger})$.

The color factors are given in Table III. To fix our notation, diagrams 1–4 have color structure 345, diagrams 5–7 have color structure [3,4]5 where [3,4] is the usual commutator, [3,4]=34−43, diagrams 8–10 have color structure 5[3,4] and diagrams 11–12 have color structure [[3,4],5].

The production of four quarks and one gluon

$$e^-(p_1,\lambda) + e^+(p_2,-\lambda) \to g(p_3,\lambda_3) + q(p_4,\lambda_4) + \bar{q}(p_5,\lambda_5) + q(p_6,\lambda_6) + \bar{q}(p_7,\lambda_7) \quad (10)$$

is described in lowest order by twenty–four Feynman diagrams if the two quarks have different flavour (case I) and by forty–eight if their flavour is the same (case II). Twelve of the diagrams for case I are shown in fig.2, all others can be obtained with the simultaneous substitutions $\bar{q}(p_5,\lambda_5) \leftrightarrow \bar{q}(p_7,\lambda_7)$ and $q(p_4,\lambda_4) \leftrightarrow q(p_6,\lambda_6)$. The additional ones needed for identical flavour can be obtained exchanging $\bar{q}(p_5,\lambda_5)$ with $\bar{q}(p_7,\lambda_7)$ including their color quantum numbers and changing the overall sign.

The amplitude squared for these processes is:

$$\left|\overline{M}\right|^2_{q\bar{q}q'\bar{q}'g} = \frac{1}{4} g_s^3 e^2 N_3 \sum_{\{\lambda\}} \sum_{i,j=1}^{24} M_i^{\{\lambda\}} M_j^{\{\lambda\}*} C_{ij} \quad (11)$$

$$\left|\overline{M}\right|^2_{q\bar{q}q\bar{q}g} = \frac{1}{4} \frac{1}{(2!)^2} g_s^3 e^2 N_3 \sum_{\{\lambda\}} \sum_{i,j=1}^{48} M_i^{\{\lambda\}} M_j^{\{\lambda\}*} C'_{ij} \quad (12)$$

in case I and case II respectively. C_{ij} and C'_{ij} are the appropriate colour factors which can be extracted from Table IV and V.

We define the following colour structures:

$$\begin{aligned}
A_1{}^{a\ i_2 j_2}_{\ i_1 j_1} &= \left(T^a T^b\right)_{i_1 j_1} \left(T^b\right)_{i_2 j_2} \\
A_2{}^{a\ i_2 j_2}_{\ i_1 j_1} &= \left(T^b T^a\right)_{i_1 j_1} \left(T^b\right)_{i_2 j_2} \\
A_3{}^{a\ i_2 j_2}_{\ i_1 j_1} &= \left(T^b\right)_{i_1 j_1} \left(T^a T^b\right)_{i_2 j_2} \\
A_4{}^{a\ i_2 j_2}_{\ i_1 j_1} &= \left(T^b\right)_{i_1 j_1} \left(T^b T^a\right)_{i_2 j_2} \\
A_5{}^{a\ i_2 j_2}_{\ i_1 j_1} &= \left(T^b\right)_{i_1 j_1} \left(T^c\right)_{i_2 j_2} c_{abc}
\end{aligned} \quad (13)$$

(14)

and

$$B_n{}^{a\ i_2 j_2}_{\ i_1 j_1} = A_n{}^{a\ i_2 j_1}_{\ i_1 j_2}. \quad (15)$$

The color factor is given by:

$$C_{nm} = A_n{}^{a\ i_2 j_2}_{\ i_1 j_1} A^{\dagger}{}_m{}^{a\ j_2 i_2}_{\ j_1 i_1} \quad (16)$$

in case I and by analogous formulae in case II, possibly with $A_{n,m} \to B_{n,m}$.

We adopt the following shorthand notation, where in the left hand side the index i stands both for the momentum p_i and for the corresponding polarization λ_i, and $[i]$

stands for the set of four indices associated with a gluon momentum and to his auxiliary momentum:

$$X(i;j;k) = X(p_i,\lambda_i;p_j;p_k,\lambda_k) \tag{17}$$

$$X([i];j) = X(p_i,\lambda_i;p_j;p_{a(i)},\lambda_i) \tag{18}$$

$$Z(i,j;k,l) = Z(p_i,\lambda_i;p_j,\lambda_j;p_k,\lambda_k;p_l,\lambda_l;1,1;1,1) \tag{19}$$

$$Z([i];j,k) = Z(p_i,\lambda_i;p_{a(i)},\lambda_i;p_j,\lambda_j;p_k,\lambda_k;1,1;1,1) \tag{20}$$

$$Z([i];[j]) = Z(p_i,\lambda_i;p_{a(i)},\lambda_i;p_j,\lambda_j;p_{a(j)},\lambda_j;1,1;1,1) \tag{21}$$

$$\begin{aligned} Z_e(i,j) &= Z(p_i,\lambda_i;p_j,\lambda_j;p_2,\lambda;p_1,\lambda;1,1;1,1)\times d_\gamma \\ &\quad + Z(i,\lambda_i;j,\lambda_j;2,\lambda;1,\lambda;c_R,c_L;c'_R,c'_L)\times d_{Z^0} \end{aligned} \tag{22}$$

where d_γ, d_{Z^0} are the photon and Z^0 propagator functions. The attachment of two external gluons to a quark line through a three–gluon vertex is conveniently described with the help of:

$$\begin{aligned} Z_2([i,j];k,l) &= Z([i];[j])\times\Big(X(k;j;l)-X(k;i;l)\Big) \\ &\quad + 2\Big(X([j];i)\times Z([i];k,l) - X([i];j)\times Z([j];k,l)\Big) \end{aligned} \tag{23}$$

The function that describes the insertion of two connected three–gluon vertices, and of the term with the same color structure in the associated four–gluon vertex, on a fermion line is:

$$\begin{aligned} &Z_3([i,j],[k];l,m) = \\ &\quad 4Z([i];l,m)\times X([j];i)\times\Big(X([k];j)+X([k];i)\Big) \\ &\quad + 2Z([k];l,m)\times\Big(Z([i];[j])\times p_i\cdot p_k \\ &\qquad +X([i];j)\times\Big(X([j];i)+2X([j];k)\Big)\Big) \\ &\quad + \Big(X(l;k;m)-X(l;i;m)-X(l;j;m)\Big)\times \\ &\qquad \Big(Z([i];[j])\times X([k];j) - 2Z([k];[j])\times X([i];j)\Big) \\ &\quad + 2X(l;j;m)\times Z([i];[j])\times\Big(X([k];j)+X([k];i)\Big) \\ &\quad - 2Z([i];l,m)\times Z([k];[j])\times p_i\cdot p_j \\ &\qquad\qquad -(i\leftrightarrow j) \end{aligned} \tag{24}$$

The denominator associated with this function is $(p_i+p_j)^2(p_i+p_j+p_k)^2$.

In order to simplify our formulae we make the convention that all repeated indices are summed over, and that the sum extends to all possible values, $\lambda = \pm 1$, of all internal helicities. The last line in eq. 26–49 gives the set of values taken independently by each momentum index. Defining the sign factors $\varepsilon(i)$ as:

$$\varepsilon(i) = \begin{cases} -1 & i = 1,2 \\ +1 & i > 2 \end{cases} \tag{25}$$

the spinor functions necessary for $q\bar{q}ggg$ production, which correspond to the diagrams shown in fig.1 are:

$$M_1 = -Z([3];6,i) \times Z([4];i,j) \times Z([5];j,k) \times Z_e(k,7) \times \varepsilon(k) \quad (26)$$
$$p_i = \{p_6, p_3\},\ \ p_j = \{p_6, p_3, p_4\},\ \ p_k = \{p_1, p_2, p_7\}$$

$$M_2 = -Z([3];6,i) \times Z([4];i,j) \times Z_e(j,k) \times Z([5];k,7) \quad (27)$$
$$p_i = \{p_6, p_3\},\ \ p_j = \{p_6, p_3, p_4\},\ \ p_k = \{p_5, p_7\}$$

$$M_3 = Z([3];6,i) \times Z_e(i,j) \times Z([4];j,k) \times Z([5];k,7) \quad (28)$$
$$p_i = \{p_6, p_3\},\ \ p_j = \{p_4, p_5, p_7\},\ \ p_k = \{p_5, p_7\}$$

$$M_4 = Z_e(6,i) \times Z([3];i,j) \times Z([4];j,k) \times Z([5];k,7) \times \varepsilon(i) \quad (29)$$
$$p_i = \{p_6, p_1, p_2\},\ \ p_j = \{p_4, p_5, p_7\},\ \ p_k = \{p_5, p_7\}$$

$$M_5 = -Z_2([3,4];6,i) \times Z([5];i,j) \times Z_e(j,7) \times \varepsilon(j) \quad (30)$$
$$p_i = \{p_6, p_3, p_4\},\ \ p_j = \{p_1, p_2, p_7\}$$

$$M_6 = -Z_2([3,4];6,i) \times Z_e(i,j) \times Z([5];j,7) \quad (31)$$
$$p_i = \{p_6, p_3, p_4\},\ \ p_j = \{p_5, p_7\}$$

$$M_7 = -Z_e(6,i) \times Z_2([3,4];i,j) \times Z([5];j,7) \times \varepsilon(i) \quad (32)$$
$$p_i = \{p_1, p_2, p_6\},\ \ p_j = \{p_5, p_7\}$$

$$M_8 = -Z([5];6,i) \times Z_2([3,4];i,j) \times Z_e(j,7) \times \varepsilon(j) \quad (33)$$
$$p_i = \{p_6, p_5\},\ \ p_j = \{p_1, p_2, p_7\}$$

$$M_9 = -Z([5];6,i) \times Z_e(i,j) \times Z_2([3,4];j,7) \quad (34)$$
$$p_i = \{p_6, p_5\},\ \ p_j = \{p_3, p_4, p_7\}$$

$$M_{10} = -Z_e(6,i) \times Z([5];i,j) \times Z_2([3,4];j,7) \times \varepsilon(i) \quad (35)$$
$$p_i = \{p_1, p_2, p_6\},\ \ p_j = \{p_3, p_4, p_7\}$$

$$M_{11} = -Z_3([3,4],[5];6,i) \times Z_e(i,7) \times \varepsilon(i) \quad (36)$$
$$p_i = \{p_1, p_2, p_7\}$$

$$M_{12} = Z_e(6,i) \times Z_3([3,4],[5];i,7) \times \varepsilon(i) \quad (37)$$
$$p_i = \{p_1, p_2, p_6\}$$

The spinor functions for the diagrams in fig.2, which describe $q\bar{q}q\bar{q}g$ production are:

$$M_{13} = Z([3];i,5)\times Z(4,i;6,j)\times Z_e(j,7)\times\varepsilon(j) \quad (38)$$
$$p_i=\{p_3,p_5\},\ \ p_j=\{p_1,p_2,p_7\}$$

$$M_{14} = -Z([3];4,i)\times Z(i,5;6,j)\times Z_e(j,7)\times\varepsilon(j) \quad (39)$$
$$p_i=\{p_3,p_4\},\ \ p_j=\{p_1,p_2,p_7\}$$

$$M_{15} = -Z([3];i,5)\times Z(4,i;j,7)\times Z_e(6,j)\times\varepsilon(j) \quad (40)$$
$$p_i=\{p_3,p_5\},\ \ p_j=\{p_1,p_2,p_6\}$$

$$M_{16} = Z([3];4,i)\times Z(i,5;j,7)\times Z_e(6,j)\times\varepsilon(j) \quad (41)$$
$$p_i=\{p_3,p_4\},\ \ p_j=\{p_1,p_2,p_6\}$$

$$M_{17} = -Z(6,i;4,5)\times Z([3];i,j)\times Z_e(j,7)\times\varepsilon(j) \quad (42)$$
$$p_i=\{p_4,p_5,p_6\},\ \ p_j=\{p_1,p_2,p_7\}$$

$$M_{18} = -Z(6,i;4,5)\times Z_e(i,j)\times Z([3];j,7) \quad (43)$$
$$p_i=\{p_4,p_5,p_6\},\ \ p_j=\{p_3,p_7\}$$

$$M_{19} = -Z_e(6,i)\times Z(i,j;4,5)\times Z([3];j,7)\times\varepsilon(i) \quad (44)$$
$$p_i=\{p_1,p_2,p_6\},\ \ p_j=\{p_3,p_7\}$$

$$M_{20} = -Z([3];6,i)\times Z(i,j;4,5)\times Z_e(j,7)\times\varepsilon(j) \quad (45)$$
$$p_i=\{p_3,p_6\},\ \ p_j=\{p_1,p_2,p_7\}$$

$$M_{21} = -Z([3];6,i)\times Z_e(i,j)\times Z(j,7;4,5) \quad (46)$$
$$p_i=\{p_3,p_6\},\ \ p_j=\{p_4,p_5,p_7\}$$

$$M_{22} = -Z_e(6,i)\times Z([3];i,j)\times Z(j,7;4,5)\times\varepsilon(i) \quad (47)$$
$$p_i=\{p_1,p_2,p_6\},\ \ p_j=\{p_4,p_5,p_7\}$$

$$\begin{aligned} M_{23} = {} & Z_e(6,i)\times\Big(2\Big(X([3];4)+X([3];5)\Big)\times Z(i,7;4,5) \\ & -2X(4;3;5)\times Z([3];i,7) \\ & -\Big(X(i;4;7)+X(i;5;7)-X(i;3;7)\Big)\times Z([3];4,5)\Big)\times\varepsilon(i) \\ & p_i=\{p_1,p_2,p_6\} \end{aligned} \quad (48)$$

$$\begin{aligned} M_{24} = {} & -Z_e(i,7)\times\Big(2\Big(X([3];4)+X([3];5)\Big)\times Z(6,i;4,5) \\ & -2X(4;3;5)\times Z([3];6,i) \\ & -\Big(X(6;4;i)+X(6;5;i)-X(6;3;i)\Big)\times Z([3];4,5)\Big)\times\varepsilon(i) \\ & p_i=\{p_1,p_2,p_7\} \end{aligned} \quad (49)$$

From the examples above the one can to construct the full amplitudes for $5j$ and $4j\gamma$ production with little effort.

Results

Our results are presented in fig.3 and 4. In fig.3 we show the total cross section for five–jet production as a function of y_{cut} in the JADE scheme [12] and in the DURHAM scheme [13]. We have neglected the mass of the quarks of the first two generations, and have summed over all their contributions. The cross section for four b–quark plus one gluon–jet production is given by the dotted lines. The dashed lines represent the cross section for the production of two b–quarks plus any combination of three light–parton jets. Finally the sum of all contributions to five–jet production including only light, strongly interacting, particles is shown by the continuous line. It is to be noticed that, at least in the JADE scheme in which y, neglecting the mass of the light hadrons which are effectively detected, represents an actual invariant mass, there is a natural lower limit to the allowed range in y_{cut} for b–quark production, which corresponds to the invariant mass of the b, $y_{cut}^{\min} \approx (m_b/M_{Z^0})^2 \approx 3 \times 10^{-3}$. At lower y_{cut} one begins to resolve the decay products of the heavy quark.

In fig.3 we also give, in the JADE scheme, the cross section for $e^+e^- \to q\bar{q}gg\gamma$, summing over five flavours. In this case we have taken for the c–quark $m_c = 1.7$ GeV. Additional cuts are necessary in order to screen our results from the collinear singularities due to initial state radiation. We have required $p_t^\gamma > 5$ GeV and $|\cos\theta_\gamma| < .72$; these cuts are similar to the selection criteria adopted by the LEP collaborations.

When our results for five–jet production are compared with the data presented by ALEPH [1] and OPAL [2] it is clear that the absolute normalization is about a factor of five too small. The simplest explanation for this discrepancy is our choice for α_s. In fact we have used $\alpha_s = .115$ which corresponds to $Q^2 = M_{z^0}^2$ with $\Lambda_{\overline{MS}} = 200$ MeV with five active flavours in the standard formula:

$$\alpha_s(Q) = \frac{1}{b_0 \log(Q^2/\Lambda^2)} \left[1 - \frac{b_1 \log(\log(Q^2/\Lambda^2))}{b_0^2 \log(Q^2/\Lambda^2)}\right] \tag{50}$$

The analysis of shape variables and jet rates to $\mathcal{O}(\alpha_s^2)$ has shown that, in order to get agreement between the data and the theoretical predictions, the scale of the strong coupling constant has to be chosen to be $Q = x_\mu M_{Z^0}$, with $x_\mu \approx 0.1$ [2]. It has later been shown that when the relevant logarithms are properly resummed [14] agreement is obtained for much larger values of the scale, $x_\mu \approx 1$. [15]. It therefore not surprising that our tree level expressions require a relatively small scale in order to describe the data. A related issue, for processes with massive quarks, is the choice of the scale of the running mass. Within our tree–level approach we have i gnored this problem, using $m_b = 5.$ GeV.

The cross section for $2b3$j is quite large, of the order of several hundreds pb at $y_{cut} = .001$ in the DURHAM scheme and $y_{cut} = .005$ in the JADE scheme, and it remains sizable out to $y_{cut} \approx .01$ and to $y_{cut} \approx .02$ respectively. Over this limited range $\sigma(y_{cut})$ decreases by more than one order of magnitude. This behaviour should be clearly observable with an efficiency of order .3 for detecting each b–quark. It will be more difficult to detect the production of $4b$j, whose cross section is only a few pb at the lowest values of y_{cut} considered in this paper.

In fig.4 we present the cross section ratios $\sigma(2b3g)/\sigma(2d3g)$ (continuous line), $\sigma(2u2bg)/\sigma(2u2dg)$ (dashed line) and $\sigma(2d2bg)/\sigma(2d2sg)$ (dotted line) in the two recombination schemes

as a function of y_{cut}. These curves confirm our previous conclusions that mass effects increase with the number of final state light partons. The ratio for the dominant $2q3g$ production process is equal to .58 at $y_{cut} = .001$ in the DURHAM scheme and to .67 at $y_{cut} = .005$ in the JADE scheme. It is even smaller for the processes with four quark jets in the final state. This corresponds to a $6 \div 8\%$ decrease in the predictions for the total five–jet cross section.

An estimate of the effects due to the *charm* mass can be obtained from the ratio $\sigma(2c2g\gamma)/\sigma(2u2g\gamma)$ which is equal to .93 at $y_{cut} = .005$ in the JADE scheme. The corresponding value for $\sigma(2b2g\gamma)/\sigma(2d2g\gamma)$ is .63, slightly smaller than in the case of $2q3g$ production.

Five–jet production will be visible also at higher energies. At $\sqrt{s} = 200$ GeV we obtain $\sigma(e^+e^- \to d\bar{d}3g) = 9.8 \times 10^{-2}\ pb$ and $\sigma(e^+e^- \to b\bar{b}3g) = 8.8 \times 10^{-2}\ pb$, showing that the mass of the b decreases the cross section by 10% even at the highest energy envisaged for LEP II.

Conclusions

The cross section for the production of b–quarks in five–jet events has been computed using helicity amplitudes and the Z–function formalism. The differences with the corresponding massless rates and the total cross sections for $2b3j$ and $4bj$ production have been studied at the Z^0 peak. Mass effects result in a $30 \div 40\%$ reduction on individual cross sections and in a $6 \div 8\%$ reduction of the total five jet production. The production of a hard photon in association with four jets has been investigated.

Acknowledgements

We gratefully acknowledge the collaboration of S. Moretti in checking the amplitudes for purely hadronic final states and the collaboration of M. Ughetti for the calculation of the processes with a hard photon.

References

[1] L3 Collaboration, B. Adeva *et al.*, Z. Phys. **C 55** (1992) 39.
ALEPH Collaboration, D. Buskulic *et al.*, Z. Phys. **C 55** (1992) 209.

[2] DELPHI Collaboration, P. Abreu *et al.*, Z. Phys. **C 54** (1992) 55.
OPAL Collaboration, P.D. Acton *et al.*, Z. Phys. **C 55** (1992) 1.

[3] L3 Collaboration, B. Adeva *et al.*, Phys. Lett. **B271** (1991) 461.
DELPHI Collaboration, P. Abreu *et al.*, Phys. Lett. **B307** (1993) 221.
OPAL Collaboration, R. Akers *et al.*, Preprint CERN-PPE/93-118, July 1993.

[4] A. Ballestrero, E. Maina and S. Moretti, Phys. Lett. **B294** (1992) 425.

[5] A. Ballestrero, E. Maina and S. Moretti, Torino Preprint DFTT 53-92, October 1992. To appear in Nucl. Phys. B.

[6] N.K. Falck, D. Graudenz and G. Kramer, Nucl. Phys. **B328** (1989) 317.

[7] N. Brown, Z. Phys. **C 51** (1991) 107.

[8] R. Kleiss and W.J. Stirling, Nucl. Phys. **B262** (1985) 235.

[9] C. Mana and M. Martinez, Nucl. Phys. **B287** (1987) 601.

[10] K. Hagiwara and D. Zeppenfeld, Nucl. Phys. **B274** (1986) 1.

[11] *Mathematica* is a registered trademark of Wolfram Research, Inc.
S. Wolfram, *Mathematica*, Addison-Wesley, Redwood City, California, 1991.

[12] JADE Collaboration, W. Bartel *et al.*, Z. Phys. **C 33** (1986) 23.
JADE Collaboration, S. Bethke *et al.*, Phys. Lett. **B213** (1988) 235.

[13] N. Brown and W.J. Stirling, Phys. Lett. **B252** (1990) 657; Z. Phys. **C 53** (1992) 629.

[14] S. Catani, L. Trentadue, G. Turnock and B.R. Webber, Phys. Lett. **B263** (1991) 491.
S. Catani, L. Trentadue, G. Turnock and B.R. Webber, Preprint CERN-TH.6640/92.
S. Catani, G. Turnock and B.R. Webber, Phys. Lett. **B272** (1991) 368.
S. Catani, G. Turnock and B.R. Webber, Phys. Lett. **B295** (1992) 269.
G. Turnock, Cambridge Preprint Cavendish-HEP-92/3; Ph.D. Thesis, U. of Cambridge (1992).
J.C. Collins and D.E. Soper, Nucl. Phys. **B193** (1981) 381.
J.C. Collins and D.E. Soper, Nucl. Phys. **B197** (1982) 446, Err. Nucl. Phys. **B213** (1983) 545.
J.C. Collins and D.E. Soper, Nucl. Phys. **B284** (1987) 253.

J. Kodaira and L. Trentadue, Phys. Lett. **B112** (1982) 66.
R. Fiore, A. Quartarolo and L. Trentadue, Phys. Lett. **B294** (1992) 431.
S. Catani, Yu.L. Dokshitzer, M. Olsson, G. Turnock and B.R. Webber, Phys. Lett. **B269** (1991) 432.
S. Catani, Yu.L. Dokshitzer, F. Fiorani and B.R. Webber, Nucl. Phys. **B377** (1992) 445.

[15] OPAL Collaboration, P.D. Acton *et al.*, Preprint CERN-PPE/93-38, March 1993.
DELPHI Collaboration, P. Abreu *et al.*, Preprint CERN-PPE/93-43, March 1993.

Table Captions

table I The Z–functions for all independent helicity combinations in terms of the functions s, t, η and μ defined in the text. The remaining Z–functions can be obatined changing sign to the helicities and exchanging $+$ with $-$, s with t and R with L.

table II The X–functions for the two independent helicity combinations in terms of the functions s, t, η and μ defined in the text. The remaining X–functions can be obatined changing sign to the helicities and exchanging $+$ with $-$, s with t and R with L.

table III The color factors, multiplied by 9, for $e^+e^- \to q\bar{q}ggg$.

table IV The color factors, multiplied by 9, for $e^+e^- \to q_1\bar{q}_1q_2\bar{q}_2$.

table V The additional color factors, multiplied by 9, needed for quarks of identical flavour $e^+e^- \to q\bar{q}q\bar{q}$.

Figure Captions

Fig. 1 Representative diagrams contributing to $e^+e^- \to q\bar{q}ggg$. All others diagrams can be obtained through permutations of the gluon labels. The contribution of the two diagrams involving a four–gluon vertex, which are not shown, are inluded in the analytical expression given in the text for the diagrams with two connected three–gluon vertices.

Fig. 2 Representative diagrams contributing to $e^+e^- \to q\bar{q}q\bar{q}$. The remaining diagrams can be obtained through simultaneous substitutions $\bar{q}(p_5, \lambda_5) \leftrightarrow \bar{q}(p_7, \lambda_7)$ and $q(p_4, \lambda_4) \leftrightarrow q(p_6, \lambda_6)$. The additional ones needed for identical flavour can be obtained exchanging $\bar{q}(p_5, \lambda_5)$ with $\bar{q}(p_7, \lambda_7)$ including their color quantum numbers and changing the overall sign.

Fig. 3 Total cross section as a function of y_{cut} in the JADE and in the DURHAM scheme for four b–quarks plus one gluon–jet production (dotted line), for the production of two b–quarks plus any combination of three light–parton jets (dashed line), and for the sum of all contributions to fiv–jet production including only light partons (continuous line).

Fig. 4 Ratio of massive to massless cross sections for $\sigma(2b3g)/\sigma(2d3g)$ (continuous line), $\sigma(2u2bg)/\sigma(2u2dg)$ (dashed line) and $\sigma(2d2bg)/\sigma(2d2sg)$ (dotted line) in the JADE and DURHAM recombination schemes as a function of y_{cut}.

$\lambda_1\lambda_2\lambda_3\lambda_4$	$Z(p_1,\lambda_1;p_2,\lambda_2;p_3,\lambda_3;p_4,\lambda_4;c_R,c_L;c'_R,c'_L)$
$++++$	$-2[s(3,1)\,t(4,2)c'_Rc_R-\mu_1\mu_2\eta_3\eta_4c'_Rc_L-\eta_1\eta_2\mu_3\mu_4c'_Lc_R]$
$+++-$	$-2\eta_2c_R[s(4,1)\mu_3c'_L-s(3,1)\mu_4c'_R]$
$++-+$	$-2\eta_1c_R[t(2,3)\mu_4c'_L-t(2,4)\mu_3c'_R]$
$+-++$	$-2\eta_4c'_R[s(3,1)\mu_2c_R-s(3,2)\mu_1c_L]$
$++--$	$-2[s(1,4)\,t(2,3)c'_Lc_R-\mu_1\mu_2\eta_3\eta_4c'_Lc_L-\eta_1\eta_2\mu_3\mu_4c'_Rc_R]$
$+-+-$	0
$+--+$	$-2[\mu_1\mu_4\eta_2\eta_3c'_Lc_L+\mu_2\mu_3\eta_1\eta_4c'_Rc_R-\mu_2\mu_4\eta_1\eta_3c'_Lc_R-\mu_1\mu_3\eta_2\eta_4c'_Rc_L]$
$+---$	$-2\eta_3c'_L[s(2,4)\mu_1c_L-s(1,4)\mu_2c_R]$

Table I

$\lambda_1\lambda_3$	$X(p_1,\lambda_1;p_2;p_3,\lambda_3)$
$++$	$(\mu_1\eta_2+\mu_2\eta_1)(\mu_3\eta_2+\mu_2\eta_3)+s(1,2)\,t(2,3)$
$+-$	$(\mu_1\eta_2+\mu_2\eta_1)s(2,3)+(\mu_2\eta_3+\mu_3\eta_2)s(1,2)$

Table II

	345	453	534	543	354	435
345	64	1	1	10	-8	-8
453	1	64	1	-8	10	-8
534	1	1	64	-8	-8	10
543	10	-8	-8	64	1	1
354	-8	10	-8	1	64	1
435	-8	-8	10	1	1	64

Table III

	A_1	A_2	A_3	A_4	A_5
A_1	24	-3	-6	21	-27
A_2	-3	24	21	-6	27
A_3	-6	21	24	-3	27
A_4	21	-6	-3	24	-27
A_5	-27	27	27	-27	54

Table IV

	A_1	A_2	A_3	A_4	A_5
B_1	-8	1	10	1	9
B_2	1	10	1	-8	9
B_3	10	1	-8	1	-9
B_4	1	-8	1	10	-9
B_5	9	9	-9	-9	0

Table V

This figure "fig1-1.png" is available in "png" format from:

http://arXiv.org/ps/hep-ph/9311303v1

This figure "fig2-1.png" is available in "png" format from:

http://arXiv.org/ps/hep-ph/9311303v1

This figure "fig3-1.png" is available in "png" format from:

http://arXiv.org/ps/hep-ph/9311303v1

This figure "fig1-2.png" is available in "png" format from:

http://arXiv.org/ps/hep-ph/9311303v1

This figure "fig2-2.png" is available in "png" format from:

http://arXiv.org/ps/hep-ph/9311303v1

This figure "fig3-2.png" is available in "png" format from:

http://arXiv.org/ps/hep-ph/9311303v1

This figure "fig1-3.png" is available in "png" format from:

http://arXiv.org/ps/hep-ph/9311303v1

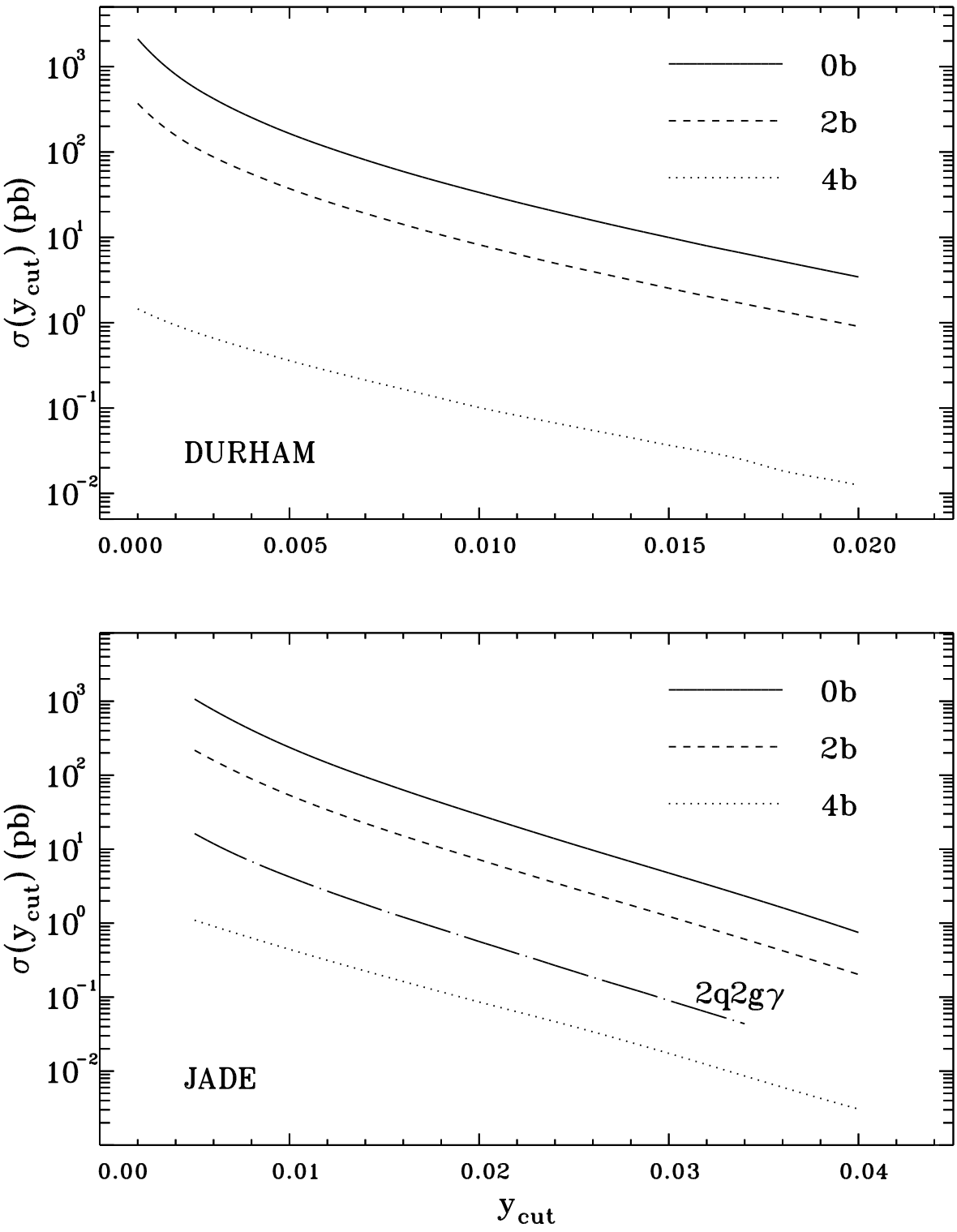
0b
2b
4b
DURHAM
$\sigma(y_{cut})$ (pb)
10^3
10^2
10^1
10^0
10^{-1}
10^{-2}
0.000
0.005
0.010
0.015
0.020
0b
2b
4b
2q2gγ
JADE
$\sigma(y_{cut})$ (pb)
0.00
0.01
0.02
0.03
0.04
y_{cut}

Fig. 3

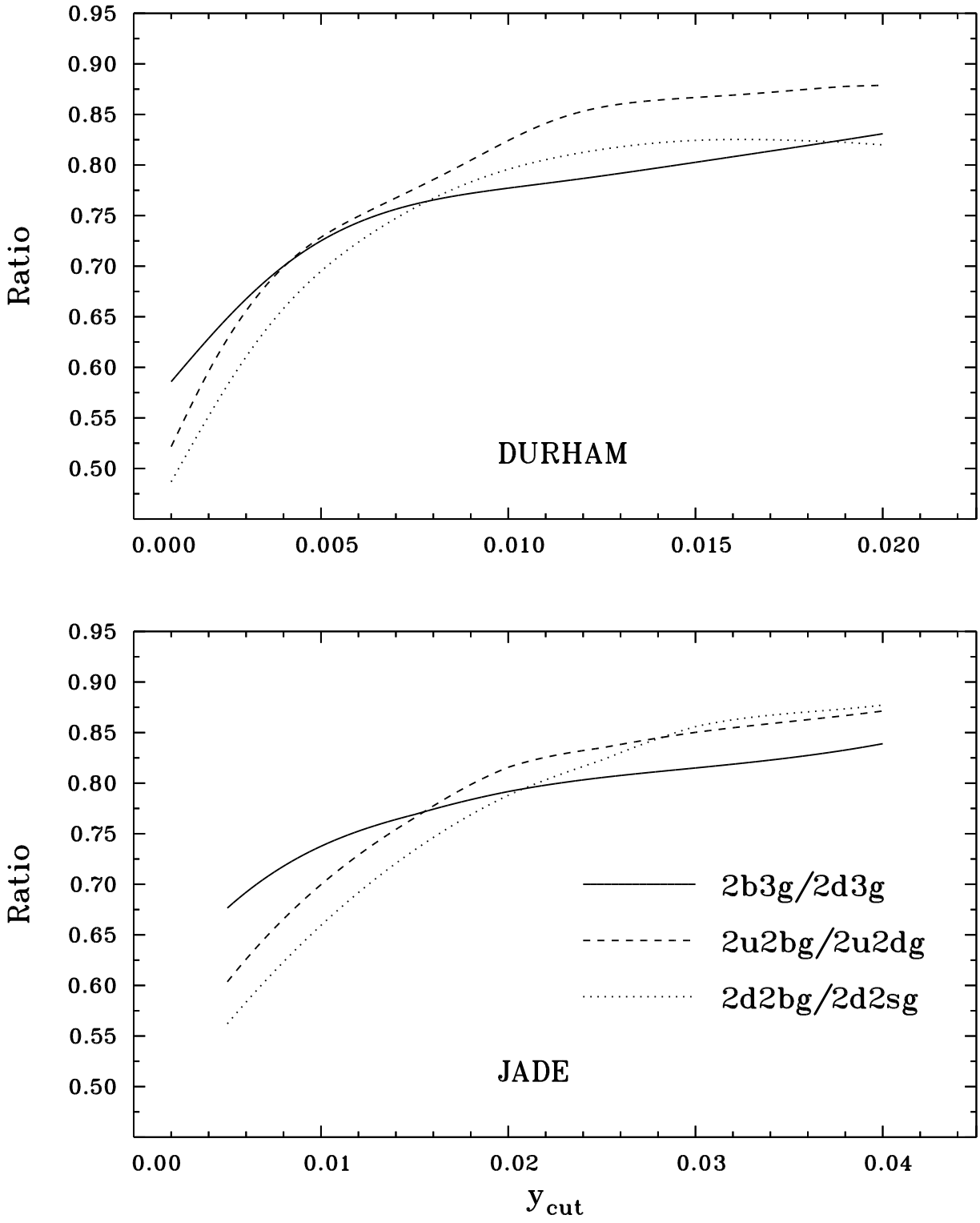
Ratio
0.95
0.90
0.85
0.80
0.75
0.70
0.65
0.60
0.55
0.50
DURHAM
0.000
0.005
0.010
0.015
0.020
Ratio
0.95
0.90
0.85
0.80
0.75
0.70
0.65
0.60
0.55
0.50
2b3g/2d3g
2u2bg/2u2dg
2d2bg/2d2sg
JADE
0.00
0.01
0.02
0.03
0.04
y_{cut}

Fig. 4